SLAC-PUB-2403
IC/HENP/79/21
November 1979
(T/E)

VECTOR MESON PRODUCTION IN HYPERCHARGE EXCHANGE REACTIONS AT 7 AND 11.5 GeV/c *

J. Ballam, J. Brau, J. Bouchez,† J. T. Carroll, C. V. Cautis,
G. B. Chadwick, V. Chaloupka, R. C. Field, D. R. Freytag, R. A. Lewis,‡
M.-N. Minard,§ K. C. Moffeit and R. A. Stevens†
Stanford Linear Accelerator Center
Stanford University, Stanford, California 94305 USA
and
P. A. Baker, J. S. Chima, P. J. Dornan, G. Hall,
T. S. Virdee‖ and A. P. White
Blackett Laboratory, Imperial College, London, England, UK

ABSTRACT

Results are presented on vector meson production in the hypercharge exchange reactions: $\pi^+p \to K^{*+}(890)Y^+$ and $K^-p \to \rho^-Y^+$ where Y^+ is either Σ^+ or $Y^{*+}(1385)$. These reactions have been studied at 7 GeV/c and 11.5 GeV/c using the SLAC Hybrid Facility. Total and differential cross sections, hyperon polarization, and vector meson decay angular distributions are presented. We find that reactions with Σ^+ production are dominated by natural parity exchange. The $Y^*(1385)$ reactions are consistent with substantial natural parity exchange contributions but also show significant unnatural parity exchange. The differential cross sections and polarization measurements for the vector meson production are compared to the pseudoscalar production reactions.

(Submitted to Nuclear Physics B.)

---

*This work was supported by the U.S. Department of Energy under contract number DE-AC03-76SF00515 and by the U.K. Science Research Council.

Present Addresses: †DPhPE/SECB,CEN-Saclay, BP No. 2, F-91190, Gif-Sur-Yvette, FRANCE.
‡Physics Department, Michigan State University, East Lansing, Michigan 48824, USA.
§Laboratoire d'Annecy de Physique des Particules, 74019-Annecy 1e Vieux, BP 909, FRANCE.
‖CERN, Geneva, SWITZERLAND.

1. INTRODUCTION

As part of a continuing study of Exchange Degeneracy (EXD) in hypercharge exchange reactions, we present data on the reactions:

$$\pi^+ p \to K^{*+}(890)\ \Sigma^+ \qquad (1)$$

$$K^- p \to \rho^-\ \Sigma^+$$

and

$$\pi^+ p \to K^{*+}(890)\ Y^{*+}(1385) \qquad (2)$$

$$K^- p \to \rho^-\ Y^{*+}(1385)$$

at 7 and 11.5 GeV/c incident momenta. We have previously presented data on the pairs of line reversed reactions [1,2]:

$$\pi^+ p \to K^+\ \Sigma^+ \qquad (3)$$

$$K^- p \to \pi^-\ \Sigma^+$$

and

$$\pi^+ p \to K^+ Y^{*+}(1385) \qquad (4)$$

$$K^- p \to \pi^- Y^{*+}(1385)$$

In a Regge picture reactions (3) and (4) are expected to be dominated asymptotically by the exchange of the same two Reggeons: the vector $K^*(890)$ and tensor $K^{**}(1420)$ [3]. Our data at 11.5 GeV/c are in agreement with weak EXD of these trajectories. In addition to natural parity exchange, reactions (1) and (2) are allowed to have contributions from unnatural parity exchange. The naturality of the exchanged system can be isolated by studying the decay angular distribution of the produced vector meson.

The present experiment is the first one to measure the four pairs of reactions (1) - (4) in a single detector at two values of incident momentum. In this paper we present differential cross-sections for the two pairs of reactions (1) and (2) and compare them to the cross sections for reactions (3) and (4) [1,2]. We have also measured the decay angular distribution of the vector meson and the polarization of the Σ^+.

In the next section we give a brief description of the experimental technique. Cross sections for reactions (1) and (2) are given in Section 3 and decay angular distributions of the vector meson and hyperon polarizations are presented in section 4. The results are discussed and compared to our published data on reactions (3) and (4) in section 5. In section 5 we also suggest a simple quark picture for reactions (1) - (4). We summarize our conclusions in section 6.

2. EXPERIMENTAL DETAILS

The experiment was conducted at the SLAC Hybrid Facility (SHF) [4]. The detector consists of the SLAC 1 m rapid cycling bubble chamber triggered by data from upstream and downstream electronic counters. The electronic data was processed on-line by a Data General NOVA 840 mini-computer. The bubble chamber was operated during the experiment at rates of up to 15 Hertz.

An electronic fast trigger was given from signals in scintillation and Čerenkov counters before and after the bubble chamber consistent with an incoming π^+ (K^-) and an outgoing fast K^+ (π^-). Downstream tracks were reconstructed on-line using thirteen planes of proportional

wire chambers (PWC). An on-line algorithm triggered the bubble chamber camera lights after eliminating low momentum tracks, interactions outside the fiducial volume and non-interacting beam tracks. For the K^- run a μ-hodoscope behind 1m of iron reduced the triggering rate from K^- decays. The detector and the trigger are described in more detail elsewhere [2,4]. The setup is shown in fig. 1 and the data taking is summarized in table I.

The film was scanned for all events with a visible strange particle decay. These events were measured in three views and reconstructed by our geometry programs. Tracks passing through the downstream system were constrained to fit the PWC data, giving a momentum resolution of $\sim$ 1.5% at 10 GeV/c.

Event and particle identification was effected by kinematic fitting and checking track ionization. In cases where there were ambiguities after checking the ionization, the higher constrained fit was taken and if ambiguities still remained, the fit with the greatest probability was selected.

The nominal sensitivities given in table I were obtained after correcting for those losses common to all reactions such as (a) interactions of the beam and outgoing trigger particle, (b) beam contamination, (c) electronic dead time, (d) detector inefficiencies and (e) losses in the trigger algorithm. Losses are similar at the two energies and values can be found in ref. [2].

To obtain cross sections, the sensitivity values quoted are further corrected for geometrical acceptance, which is dependent on the particular final state under consideration as discussed in the next section. Average acceptances over our momentum transfer range are given in table I for reactions (1) and (2).

3. CROSS SECTIONS

Differential cross sections were obtained by fitting the amount of single or double resonance production in several momentum transfer intervals. The momentum transfer range extended to $|t'| = 1(\mathrm{GeV/c})^2$, where $t' = t - t_{min}$ and t is the momentum transfer from the beam to the vector meson. In these fits a phase-space background was assumed; for reaction (2) we also included single resonance production as background. The method of analysis was similar to the one described in ref. [2].

To improve the signal to background ratio mass cuts were applied on the experimental sample. The selection criteria were taken into account in the fits to the data and in the calculation of the geometrical acceptance of the downstream system.

The mass cuts chosen are summarized below:

(i) $\pi^+ p \rightarrow K^+ \Sigma^+ \pi^o$

There is a low mass $\Sigma\pi$ peak in the 1600-1700 region which contributes substantial background under the $K^*(890)$. A mass cut $M(\Sigma\pi) \geq 1.8$ GeV/c^2 eliminates this and gives a very clear $K^*(890)$ signal shown in fig. 2(a).

(ii) $K^- p \rightarrow \pi^- \Sigma^+ \pi^o$

A similar $\Sigma\pi$ peak is observed around 1600 and is also removed by demanding $M(\Sigma\pi) \geq 1.8$ GeV/c^2. This eliminates almost all background under the ρ^- as seen in fig. 2(b).

(iii) $\pi^+ p \rightarrow K^+ \pi^+ \Lambda\pi^o$

Scatter plots of $M(\Lambda\pi^+)$ versus $M(K^+\pi^o)$ are given in figs. 3 and 4. They show associated K^* -Y^* production. The shaded histograms result from selecting K^* and Y^* events respectively. After selecting K^* events there is very little background under the $Y^*(1385)$ but there is a significant background under the $K^*(890)$ after making the Y^* selection.

(iv) $K^- p \rightarrow \pi^- \pi^+ \Lambda\pi^o$

Similar plots for this channel are shown in figs. 3 and 4. Copious Y^* production is seen and again it is found that the main background contribution is under the vector meson after making the Y^* selection.

We have estimated the geometrical acceptance of the downstream system by generating Monte Carlo events with the same decay angular distribution and the same cuts as the data (see section 4) and projecting the tracks into the downstream system. The acceptance was determined as a function of the momentum transfer and was used to correct the differential and integrated cross sections.

The cross sections are given in table II and the differential cross sections in tables III and IV and figs. 5 and 6. The errors on the integrated cross sections include an estimated 20% systematic

contribution caused by uncertainties in normalization background subtractions, and geometrical acceptances.

In fig. 7 we plot the cross sections for reactions (1) and (2) as a function of incident momentum [5]. The results from this experiment at 7 and 11.5 GeV/c are consistent with the observation [6] that the K^- induced reactions cross sections have a steeper energy dependence than the π^+ reaction cross sections.

4. DECAY ANGULAR DISTRIBUTION OF THE VECTOR MESON AND HYPERON POLARIZATION.

By measuring the complete decay of both the vector meson and the hyperon, one can estimate the elements of the joint spin density matrix in reactions (1) and (2). Because of limited statistics however, we have analyzed the vector meson and hyperon decays separately.

The decay angular distribution of the vector meson can be expressed in terms of the following linear combinations of the spin density matrix elements:

$$\begin{aligned} \rho^+_1 &= \rho_{11} + \rho_{1-1} \\ \rho^-_1 &= \rho_{11} - \rho_{1-1} \\ \rho^-_0 &= \rho_{00} \end{aligned} \qquad (5)$$

The element ρ^-_0 gives the production of vector mesons with spin projection zero, which can only be produced by unnatural parity exchange [7]. Asymptotically, ρ_1^+ (ρ_1^-) approximates the proportion of vector meson with spin projection $|1|$ produced by natural (unnatural) parity exchange [8].

With this parametrization the one dimensional distributions can be written as:

$$W(\cos\theta) = \frac{3}{4}\left[\, 2\rho_0^{-}\cos^2\theta + (\rho_1^{+} + \rho_1^{-})\sin^2\theta \,\right]$$
$$W(\phi) = \frac{1}{2\pi}\left[\, \rho_0^{-} + 2\rho_1^{+}\sin^2\phi + 2\rho_1^{-}\cos^2\phi \,\right] \qquad (6)$$

The parameters ρ_0^{-} and $\rho_1^{\pm}$ were estimated from fits to the decay angular distributions in the Jackson frame [7] in the region $-t' < 1$ $(GeV/c)^2$. The effects of cuts on the experimental sample and the geometrical acceptance were taken into account in the theoretical expressions used in the fits. We have subtracted the contribution from background under the vector meson by studying the angular distributions of the two-meson system outside the mass region of the vector meson.

The values of the density matrix elements are given in table V and the results of the fits for reactions (1) and (2) are compared to the experimental decay angular distributions in figs. 8 and 9.

The polarization of the Σ^+ hyperon in reactions (1) was estimated from the parity non-conserving decay $\Sigma^+ \to p\pi^o$ using the expression:

$$P = \frac{1}{\alpha}\,\frac{\langle\cos\theta_p\rangle}{\langle\cos^2\theta_p\rangle}$$

where α is the decay asymmetry parameter and θ_p is the angle between the proton direction in the hyperon rest frame and the normal to the production plane. The $\langle\cos^2\theta_p\rangle$ term in the denominator corrects for scanning losses of short Σ's with forward proton decays which are symmetric with respect to the production plane. Sigma polarizations

at the two momenta for reactions (1) are shown in fig. 10 as a function of momentum transfer. We also include for comparison the values obtained by this collaboration for the Σ^+ polarization in reactions (3).

5. DISCUSSION OF RESULTS

In this section we discuss our results on the cross section, Σ polarization and the decay angular distribution of the produced vector mesons. We compare the observed properties of reactions (1) and (2) with those reported by us [1,2] on reactions (3) and (4) in order to obtain a qualitative description of the family of hypercharge-exchange reactions

$$Mp \to M'Y^+$$

where $M = \pi^+$ or K^-,

M' = pseudoscalar (K^+ or π^-) or vector (K^{*+} or ρ^-) meson,

$Y^+ = \Sigma^+$ or $Y^{*+}(1385)$ hyperon.

For pseudoscalar production angular momentum conservation requires natural parity exchange. For vector production, where unnatural parity exchange is not forbidden, we estimate the natural parity exchange contribution by investigating the vector meson decays (see sec. 4).

The vector meson density matrix elements (table V) show that the reactions producing a vector meson and a Σ are dominated by natural parity exchange at both energies. The identification of the dominant production mechanism as degenerate K^*/K^{**} exchange is strengthened by additional similarities with pseudoscalar production:

(1) The differential cross sections of the π^+ and K^- induced reactions are similar in shape and absolute normalization (see fig. 5).

(2) The Σ^+ polarization (fig. 10) for the two reactions shows the same mirror-symmetric pattern as observed in corresponding pseudoscalar production. This suggests interference between Regge amplitudes with opposite signatures and degenerate trajectories but unequal residues.

The only significant difference between the vector and pseudoscalar production with the Σ^+ is an indication of a turnover at low momentum transfer in vector production, especially noticeable at 11.5 GeV/c (see fig. 5).

The analysis of vector production with a $Y^*(1385)$ (reactions (2)) is considerably more complicated. This is primarily due to uncertainties in the background subtraction and to larger corrections for geometrical acceptance. The density matrix elements in table V show that in this case production is approximately evenly split between natural and unnatural parity exchange. The apparent further suppression of natural parity exchange in reaction $K^-p \to \rho^- Y^{*+}(1385)$ at 11.5 GeV/c is not statistically convincing. The low momentum transfer behavior of the differential cross sections is also more complicated. The data do not show a clear turnover at small t' as observed in the corresponding pseudoscalar production reactions at both 7 and 11.5 GeV/c [1,2]. On the other hand, the relation of the cross sections for π^+ and K^- induced

vector meson production is similar to that observed in the reactions producing a pseudoscalar meson: The K^- induced reaction has a somewhat larger cross section, with some evidence for the difference becoming smaller at higher energy (see fig. [7] and table II).

We now discuss the systematic trends of all four reaction pairs. In fig. 11 we compare the 11.5 GeV/c differential cross sections for reaction (1)-(4). We observe a convergence of all cross sections at $-t' \geq 0.25$ $(GeV/c)^2$, while reactions (1), (2) and (4) are nearly identical also in the small t range and have developed the forward dip generally associated with helicity flip dominated reactions. We note that all four pairs of reactions discussed in this section can be illustrated by the same quark diagram (fig. 12). In each case there is a transition of the type $\bar{d} \rightarrow \bar{s}$ compared with a quark line-reversed process $s \rightarrow d$. In this model the only difference between K and K^*, or Σ and Y^*, is the spin configuration of the quarks. Therefore any reactions related by such diagrams will be candidates for EXD tests.

6. CONCLUSIONS

We have measured cross sections, spin density matrix elements of the vector meson and Σ^+ polarization for the hypercharge exchange reactions (1) and (2) at 7 and 11.5 GeV/c incident momentum. The present data were compared to our published results on pseudoscalar production in reactions (3) and (4).

We found the Σ^+ reactions (1) to be dominated by the exchange of vector and tensor K^* trajectories, similar to reactions (3) and (4). The data for all three pairs of reactions (1), (3), and (4) at 11.5 GeV/c are in agreement with weak EXD of these trajectories. Reactions (2) are also consistent with substantial natural parity exchange contributions, but experimental uncertainties are larger than in any of the other reactions. However, these $Y^*(1385)$ reactions do show significant evidence for unnatural parity exchange contributions at 7 and 11.5 GeV/c. The differential cross sections for all four pairs of reactions at 11.5 GeV/c are equal within errors for $-t' > 0.25$ $(GeV/c)^2$.

Acknowledgements

We wish to thank the staff of the Accelerator and the SLAC 1 m hybrid bubble chamber facility and the scanners and measurers at SLAC and Imperial College.

References

1. P. A. Baker et al., Phys. Rev. Lett. 40, (1978) 678, J. Ballam et al., Phys. Rev. Lett. 41, (1978) 676, P. A. Baker et al., Imperial College report IC/HENP/78/21 (1978) or Stanford Linear Accelerator Center report SLAC-PUB-2169 (1978).
2. C. V. Cautis et al., Nucl. Phys. B156, (1979) 507, P. A. Baker et al., Imperial College report IC/HENP/79/8 (1979) submitted to Nuclear Physics B.
3. F. J. Gilman, Phys. Lett. 29B, (1969) 673, R. C. Arnold, Phys. Rev. 153, (1967) 1506, K. W. Lai and J. Louie, Nucl. Phys. B19, (1970) 205.
4. G. B. Bowden et al., Nucl. Instr. and Meth. 138, (1976) 75; J. Ballam and R. Watt, Ann. Rev. Nucl. Sci. 27, (1977) 75; R. C. Field, SHF Memo 67, Stanford Linear Accelerator Center internal publication, Group BC, (1977).
5. S. Dagan et al., Phys. Rev. 161, (1967) 1384; W. Butler et al., Phys. Rev. D7, (1973) 3177; D. Toet et al., Nucl. Phys. B63, (1973) 248; W. Cooper et al., Phys. Rev. Lett. 20, (1968) 472; W. Cooper et al., Nucl. Phys. B23, (1970) 605; ABBCCLV Collaboration, Paper contributed to the XIX Int. Conf. on High Energy Physics, Tokyo, 23-30 August 1978 and private communication, J. Badier et al., Proceedings of 12th International Conference on High Energy Physics, Dubna, Vol. 1 (1964) 650; M. Hague et al., Phys. Rev. 152, (1966) 1148; A. J. deGroot et al., Nucl. Phys. B74, (1974) 77; U. E. Kruse et al., Phys. Rev. 177, (1969) 1951; M. Aderholz et al., Nucl. Phys. B11, (1969) 259; M. C. Goddard et al., Phys. Rev. D19, (1979) 1350; D. C. Colley et al., Nuovo Cimento 53A, (1968) 762; M. Aguilar-Benitez, Nucl. Phys. B124, (1977) 189.
6. W. Lohmann and H. J. Schreiber, Phys. Lett. 84B, (1979) 519.
7. K. Gottfried and J. D. Jackson, Nuovo Cimento 33, (1964) 309.
8. J. P. Ader et al., Nuovo Cimento 56A, (1968) 952.

Table I - Statistics of the experiment and average acceptance.

p(Gev)	Reaction	Pictures (millions)	Sensitivity (ev/μb)	Y^+	Average Acceptance
7	$\pi^+ p \to K^* Y^+$	0.42	150	Σ	0.65
				$Y^*(1385)$	0.60
	$K^- p \to \rho^- Y^+$	0.41	100	Σ	0.35
				$Y^*(1385)$	0.30
11.5	$\pi^+ p \to K^* Y^+$	1.20	279	Σ	0.83
				$Y^*(1385)$	0.77
	$K^- p \to \rho^- Y^+$	0.70	190	Σ	0.26
				$Y^*(1385)$	0.21

Table II - Summary of integrated cross section measurements.

The errors include 20% systematic uncertainty.

Reaction	Beam Momentum (GeV/c)	Total Cross Section (μb)	t' Range $(GeV/c)^2$
$\pi^+ p \to K^{*+}_{(890)}\ \Sigma^+$	7.0	15.6 ± 4.3	$\lvert t' \rvert \leq 0.9$
	11.5	6.7 ± 1.4	$\lvert t' \rvert \leq 1.0$
$K^- p \to \rho^-\ \Sigma^+$	7.0	20.6 ± 5.4	$\lvert t' \rvert \leq 0.9$
	11.5	6.8 ± 1.5	$\lvert t' \rvert \leq 1.0$
$\pi^+ p \to K^{*+}_{(890)}\ Y^{*+}(1385)$	7.0	9.6 ± 2.3	$\lvert t' \rvert \leq 1.0$
	11.5	5.6 ± 1.5	
$K^- p \to \rho^- Y^{*+}_{(1385)}$	7.0	13.2 ± 3.0	$\lvert t' \rvert \leq 1.0$
	11.5	8.2 ± 1.9	

Table III - Σ^+ reactions. Differential cross-sections. Only statistical errors are given.

(a) 7 GeV/c

t' $(GeV/c)^2$		$d\sigma/dt'$ $[\mu b/(GeV/c)^2]$	
		$\pi^+ p \to K^{*+}_{890}$ Σ^+	$K^- p \to \rho^-$ Σ^+
0.0	0.05	25.9 ± 9.8	52.9 ± 17.6
0.05	0.15	37.8 ± 8.2	46.0 ± 10.9
0.15	0.30	27.7 ± 5.7	38.0 ± 8.5
0.30	0.45	16.9 ± 4.9	18.0 ± 6.0
0.45	0.90	8.5 ± 2.4	11.0 ± 3.5

(b) 11.5 GeV/c

0.0	0.08	12.9 ± 2.4	9.4 ± 3.0
0.08	0.16	19.8 ± 3.0	20.2 ± 3.9
0.16	0.24	14.0 ± 2.4	20.0 ± 3.3
0.24	0.4	10.7 ± 1.3	7.9 ± 1.4
0.4	0.6	3.7 ± 0.65	5.6 ± 1.3
0.6	1.0	1.2 ± 0.26	1.05 ± 0.38

Table IV - $Y^*(1385)$ reactions: Differential cross-sections.

Only statistical errors are given.

(a) 7 GeV/c

t' $(GeV/c)^2$		$d\sigma/dt'$ $[\mu b/(GeV/c)^2]$	
		$\pi^+ p \to K^{*+}_{890}$ Y^{*+}_{1385}	$K^- p \to \rho^-$ Y^{*+}_{1385}
0.0	0.05	20.9 ± 5.8	51.0 ± 10.0
0.05	0.15	23.4 ± 4.4	30.3 ± 5.3
0.15	0.3	15.4 ± 3.1	17.6 ± 3.5
0.3	0.5	9.1 ± 2.3	12.0 ± 2.7
0.5	1.0	4.2 ± 1.2	5.2 ± 1.3

(b) 11.5 GeV/c

0.0	0.1	14.1 ± 2.5	35.7 ± 5.2
0.1	0.2	6.9 ± 1.7	16.7 ± 4.5
0.2	0.3	9.7 ± 2.0	11.9 ± 3.8
0.3	0.6	5.2 ± 0.9	4.6 ± 1.3
0.6	1.0	2.5 ± 0.6	0.94 ± 0.48

Table V - Spin density matrix elements of the vector meson in the Jackson frame. The upper index refers to the naturality of the exchange.

Reaction	p_{Beam} (GeV/c)	ρ_0^-	ρ_1^-	ρ_1^+
$\pi^+ p \to K^{*+}_{(890)} \Sigma^+$	7	0.11 ± 0.12	0.04 ± 0.07	0.85 ± 0.09
	11.5	0.10 ± 0.08	0.05 ± 0.12	0.85 ± 0.12
$K^- p \to \rho^- \Sigma^+$	7	0.05 ± 0.08	0.20 ± 0.06	0.75 ± 0.05
	11.5	0.08 ± 0.10	0.07 ± 0.18	0.85 ± 0.18
$\pi^+ p \to K^{*+}_{(890)} Y^{*+}_{(1385)}$	7	<0.15	0.44 ± 0.10	0.56 ± 0.10
	11.5	0.12 ± 0.12	0.30 ± 0.15	0.58 ± 0.15
$K^- p \to \rho^- Y^{*+}_{(1385)}$	7	0.19 ± 0.15	0.34 ± 0.10	0.47 ± 0.13
	11.5	0.40 ± 0.12	0.31 ± 0.16	0.29 ± 0.16

Figure Captions

Fig. 1. Layout of the SLAC hybrid facility. The rapid cycling bubble chamber is the cylinder shown in a cut-away drawing of its magnet body. Steel hadron filters used in the K^- exposure are shown in front of S4 and S5. The beam is incident from the left foreground.

Fig. 2. Reactions $\pi^+p \to K^+\pi^o\Sigma^+$ and $K^-p \to \pi^-\pi^o\Sigma^+$: Invariant mass distributions for the $K^+\pi^o$ and $\pi^-\pi^o$ system at 7 and 11.5 GeV. Events were selected with $M_{\pi^o\Sigma^+} > 1.8$ GeV/c^2 and $|t| < |(\text{GeV/c})^2$.

Fig. 3. Reactions $\pi^+p \to K^+\pi^o\Lambda\pi^+$ and $K^-p \to \pi^-\pi^o\Lambda\pi^+$: Scatter plot of the $K^+\pi^o$ and $\pi^-\pi^o$ versus the $\Lambda\pi^+$ invariant masses at 7 GeV/c.

Fig. 4. Reactions $\pi^+p \to K^+\pi^o\Lambda\pi^+$ and $K^-p \to \pi^-\pi^o\Lambda\pi^+$: Scatter plot of the $K^+\pi^o$ and $\pi^-\pi^o$ versus the $\Lambda\pi^+$ invariant masses at 11.5 GeV/c.

Fig. 5. Differential cross sections for the $\pi^+p \to K^{*+}(890)\Sigma^+$ and $K^-p \to \rho^-\Sigma^+$ reactions at a) 7 GeV/c and b) 11.5 GeV/c.

Fig. 6. Differential cross sections for the $\pi^+p \to K^{*+}(890)\ Y^{*+}(1385)$ and $K^-p \to \rho^-Y^{*+}(1385)$ at a) 7 GeV/c and b) 11.5 GeV/c.

Fig. 7. Momentum dependence of the reactions $\pi^+p \to K^{*+}(890)Y^+$ and $K^-p \to \rho^-Y^+$. The data from other experiments are from ref. [5].

Fig. 8. Vector meson decay angular distributions for the Σ reactions in the Jackson frame at a) 7 GeV/c and b) 11.5 GeV/c. The solid line is the result of the fit.

Fig. 9. Vector meson decay angular distributions for the Y* reactions in the Jackson frame at a) 7 GeV/**c** and b) 11.5 GeV/c. The solid line is the result of the fit.

Fig. 10. Polarization of Σ^+ at a) 7 GeV/c and b) 11.5 GeV/c.

Fig. 11. Comparison of differential cross section for reactions (1)-(4) at 11.5 GeV/c. For clarity the results for reactions (3) and (4) are represented by smooth curves approximating the data points. The lines for reactions (4) are results of minimum χ^2 fits to the data.

Fig. 12 Quark line diagram for reactions (1) - (4).

SLAC HYBRID FACILITY

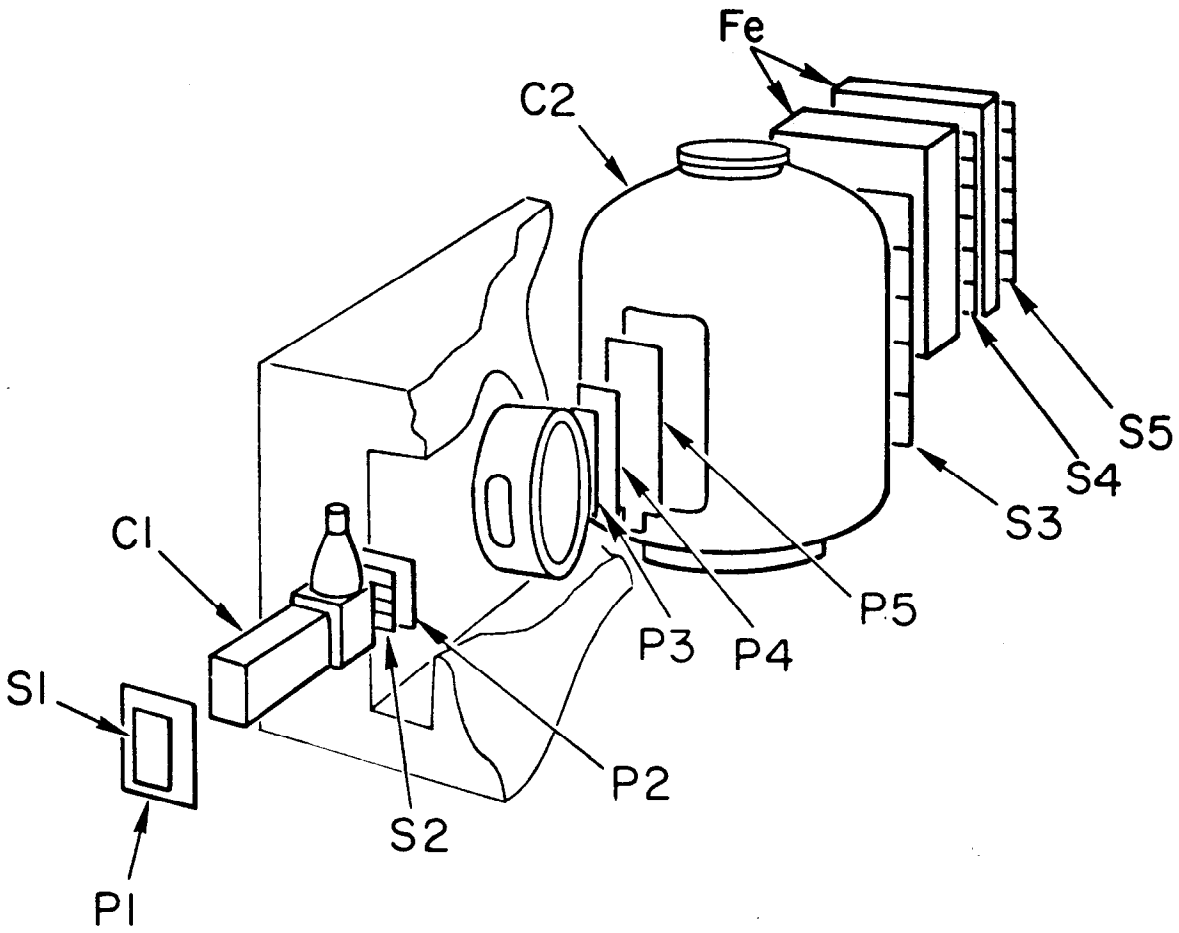

S1 Beam Scintillator
S2-5 Hodoscopes
C1-2 Cerenkov Counters
P1-5 P.W.C.s

9 - 78

3460A7

Fig. 1

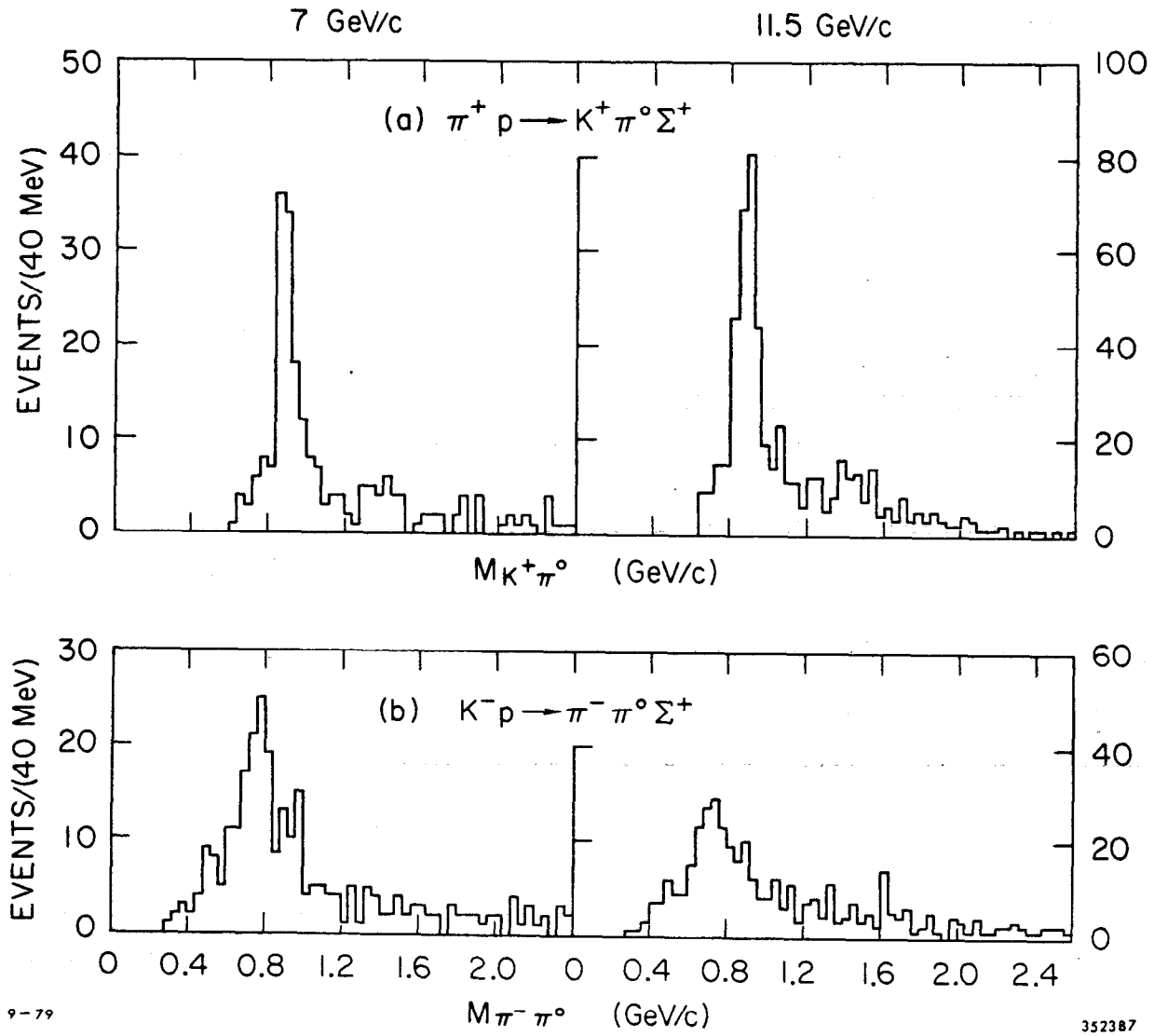
7 GeV/c
11.5 GeV/c
(a) $\pi^+ p \rightarrow K^+ \pi^\circ \Sigma^+$
EVENTS/(40 MeV)
$M_{K^+\pi^\circ}$ (GeV/c)
(b) $K^- p \rightarrow \pi^- \pi^\circ \Sigma^+$
EVENTS/(40 MeV)
$M_{\pi^-\pi^\circ}$ (GeV/c)
9-79
352387

Fig. 2

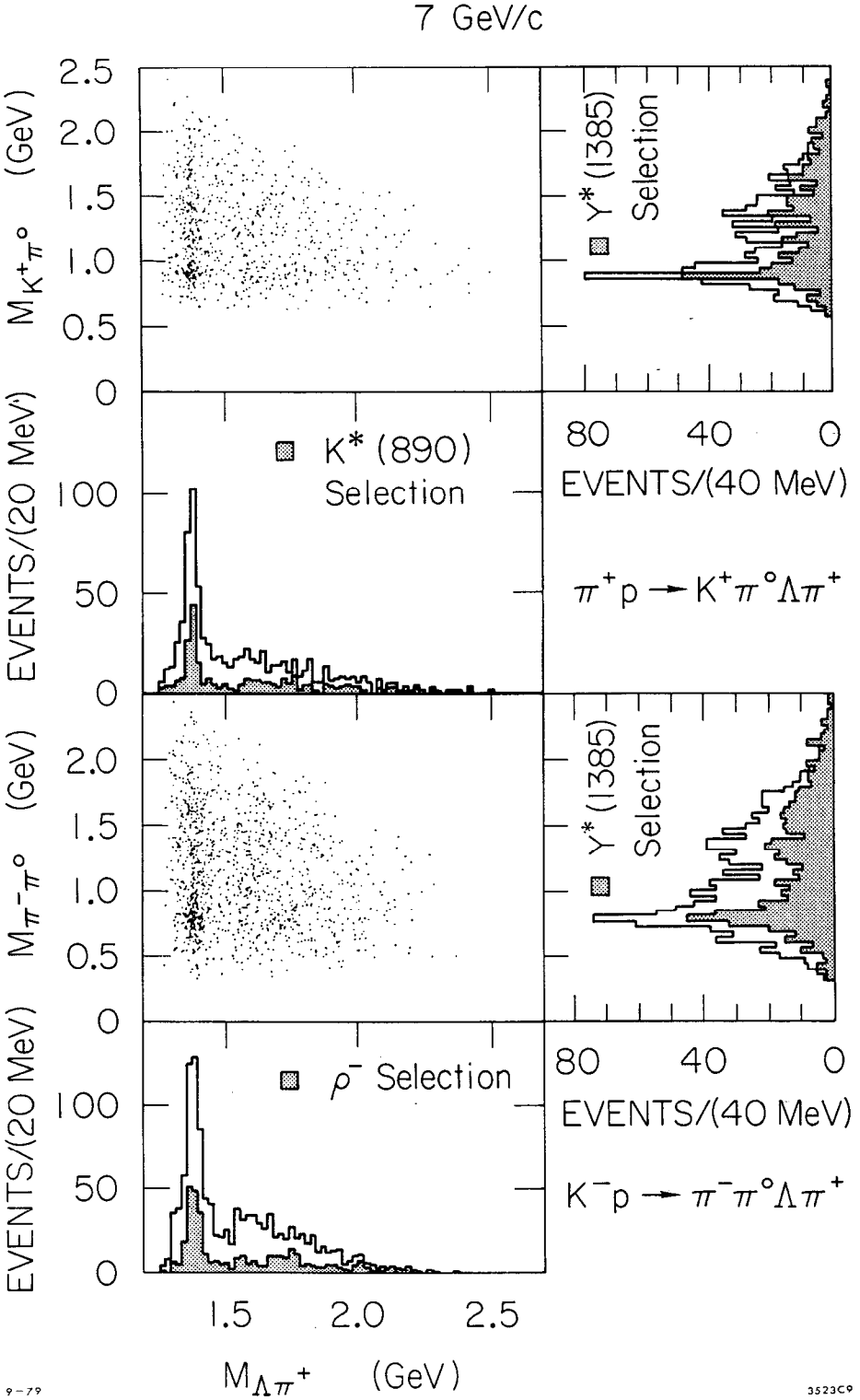
7 GeV/c
$M_{K^+\pi^\circ}$ (GeV)
EVENTS/(20 MeV)
K* (890) Selection
Y* (1385) Selection
EVENTS/(40 MeV)
$\pi^+ p \rightarrow K^+ \pi^\circ \Lambda \pi^+$
$M_{\pi^-\pi^\circ}$ (GeV)
ρ^- Selection
$K^- p \rightarrow \pi^- \pi^\circ \Lambda \pi^+$
$M_{\Lambda\pi^+}$ (GeV)
9-79
3523C9

Fig. 3

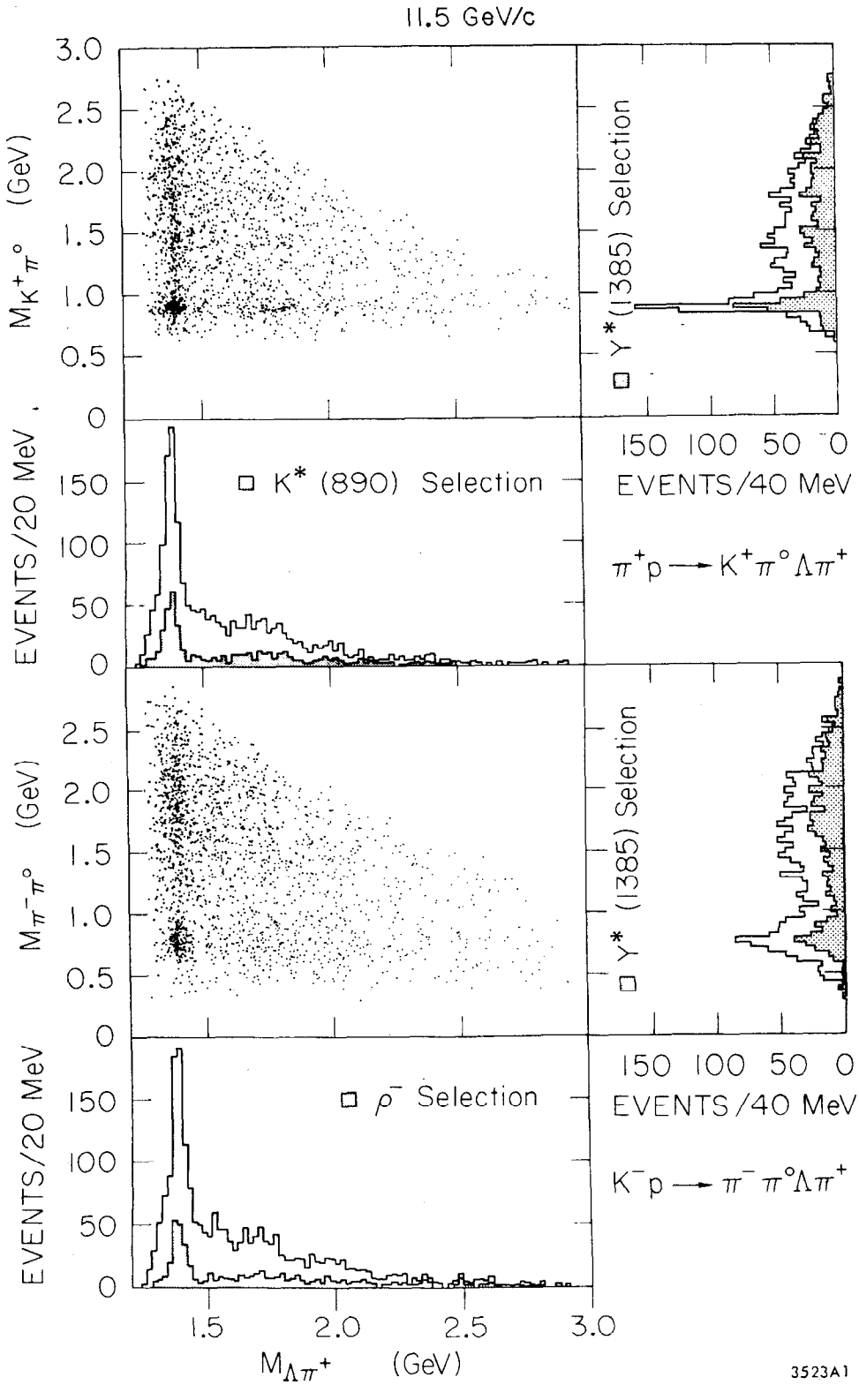
11.5 GeV/c
$M_{K^+\pi^\circ}$ (GeV)
EVENTS/20 MeV
□ K* (890) Selection
□ Y*(1385) Selection
EVENTS/40 MeV
$\pi^+ p \rightarrow K^+ \pi^\circ \Lambda \pi^+$
$M_{\pi^-\pi^\circ}$ (GeV)
□ ρ⁻ Selection
$K^- p \rightarrow \pi^- \pi^\circ \Lambda \pi^+$
$M_{\Lambda\pi^+}$ (GeV)
3523A1

Fig. 4

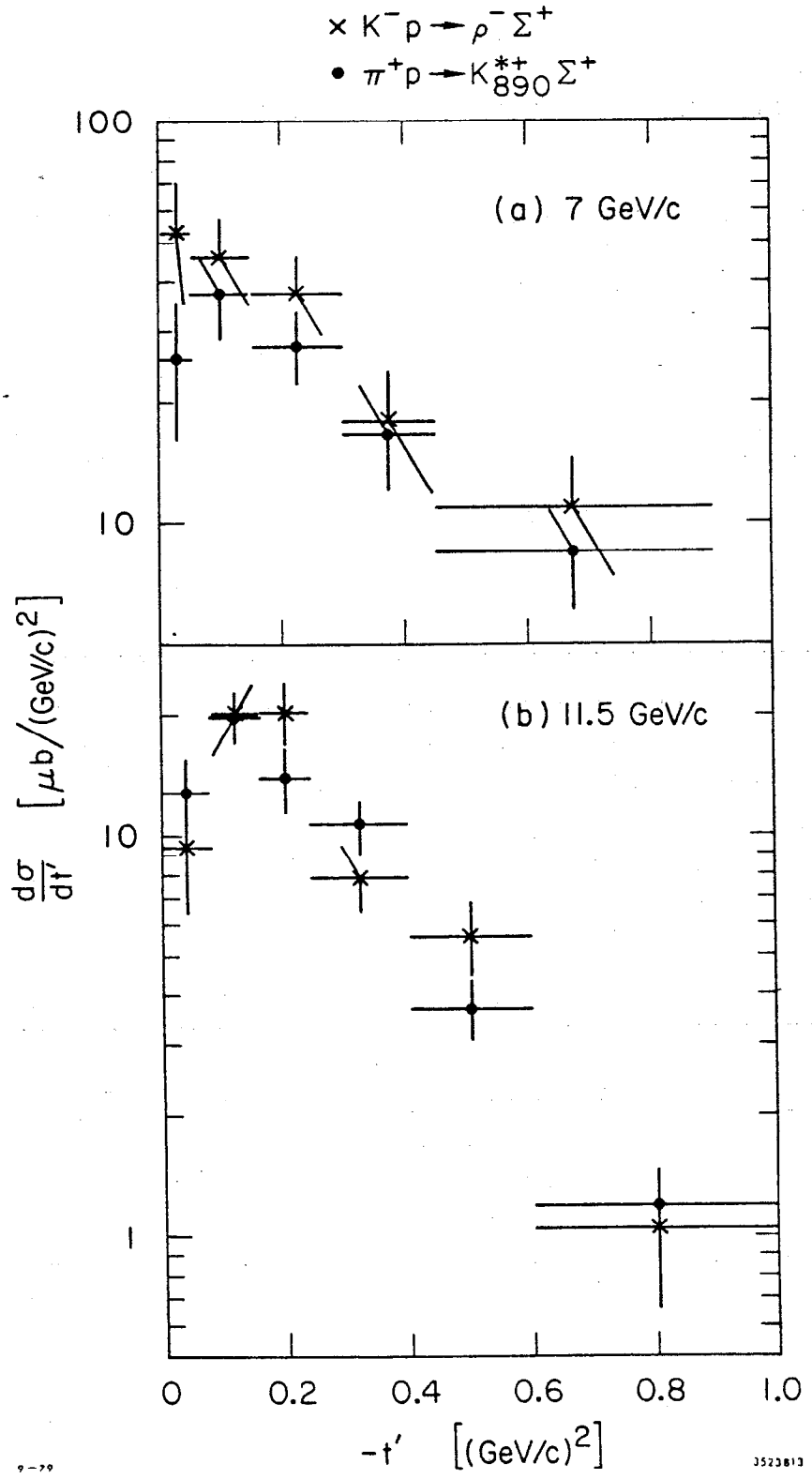
× K⁻p → ρ⁻Σ⁺
• π⁺p → K*⁺₈₉₀Σ⁺
100
10
(a) 7 GeV/c
(b) 11.5 GeV/c
10
1
dσ/dt' [μb/(GeV/c)²]
0
0.2
0.4
0.6
0.8
1.0
-t' [(GeV/c)²]
9-79
3523813

Fig. 5

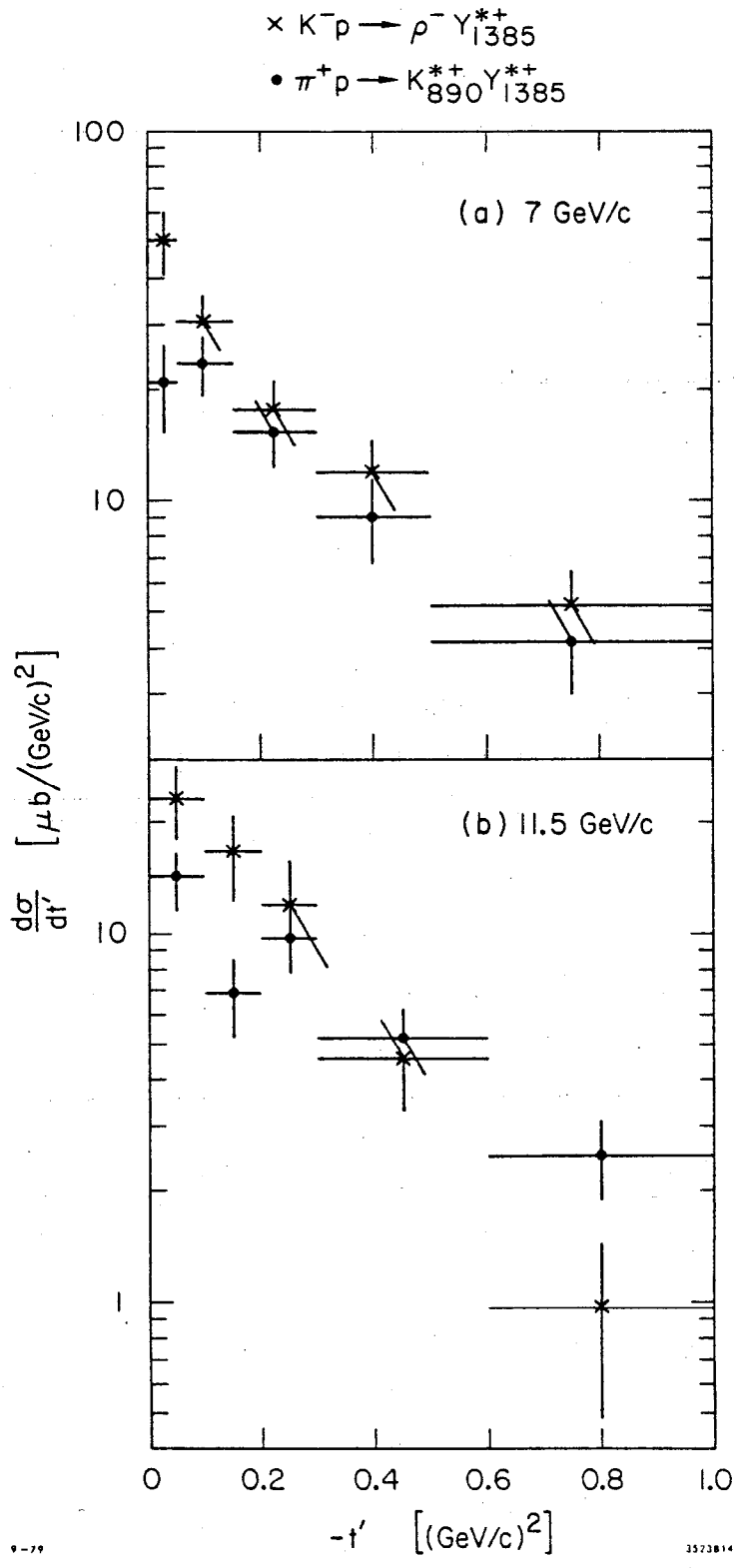
× K⁻p → ρ⁻ Y*++1385
• π⁺p → K*++890 Y*++1385
(a) 7 GeV/c
(b) 11.5 GeV/c
100
10
10
1
dσ/dt' [μb/(GeV/c)²]
0
0.2
0.4
0.6
0.8
1.0
-t' [(GeV/c)²]
9-79
3573B14

Fig. 6

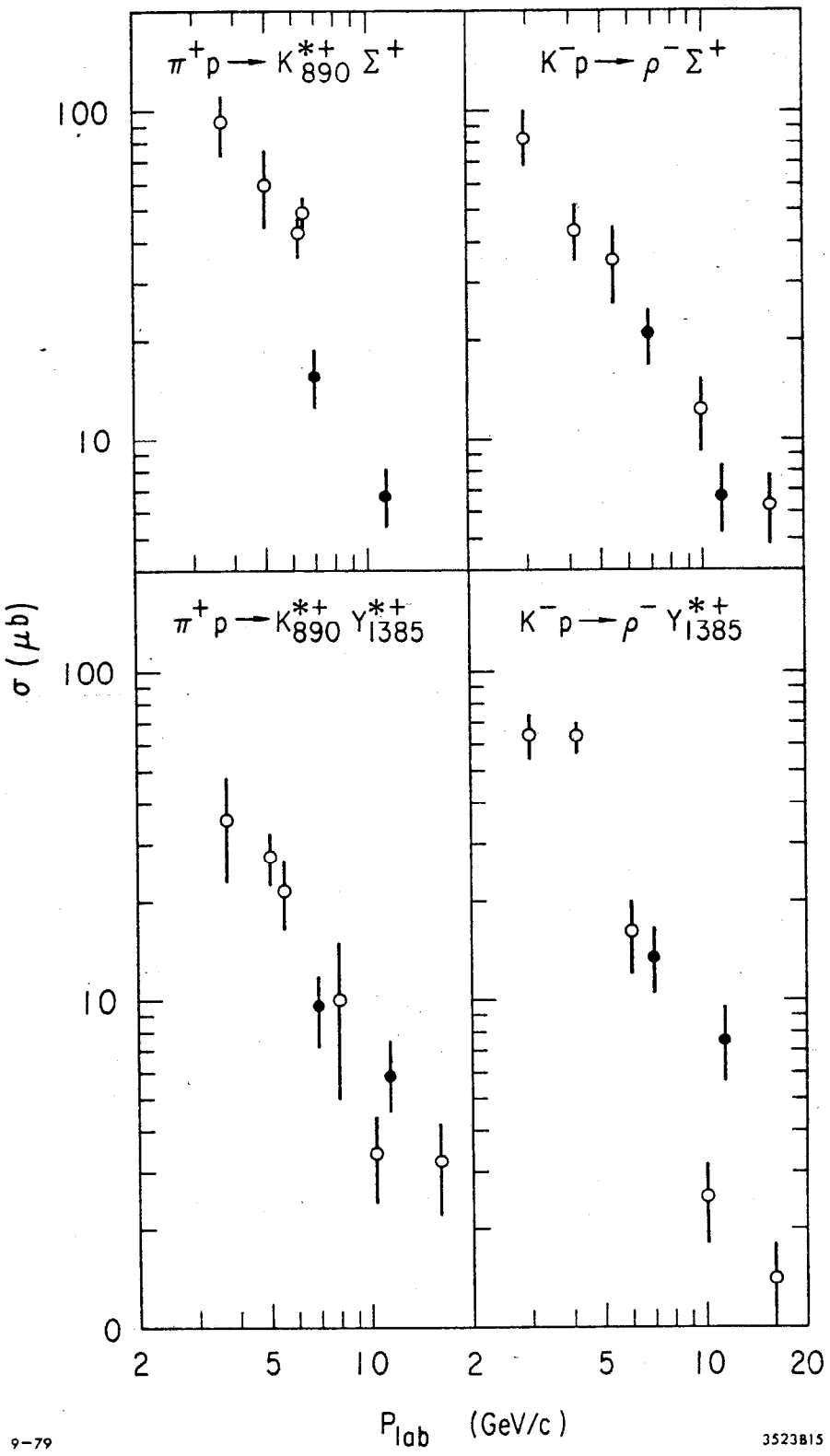
$\pi^+ p \rightarrow K^{*+}_{890}\,\Sigma^+$
$K^- p \rightarrow \rho^-\,\Sigma^+$
$\pi^+ p \rightarrow K^{*+}_{890}\,Y^{*+}_{1385}$
$K^- p \rightarrow \rho^-\,Y^{*+}_{1385}$
100
10
100
10
0
$\sigma\,(\mu b)$
2
5
10
2
5
10
20
P_{lab} (GeV/c)
9-79
3523B15

Fig. 7

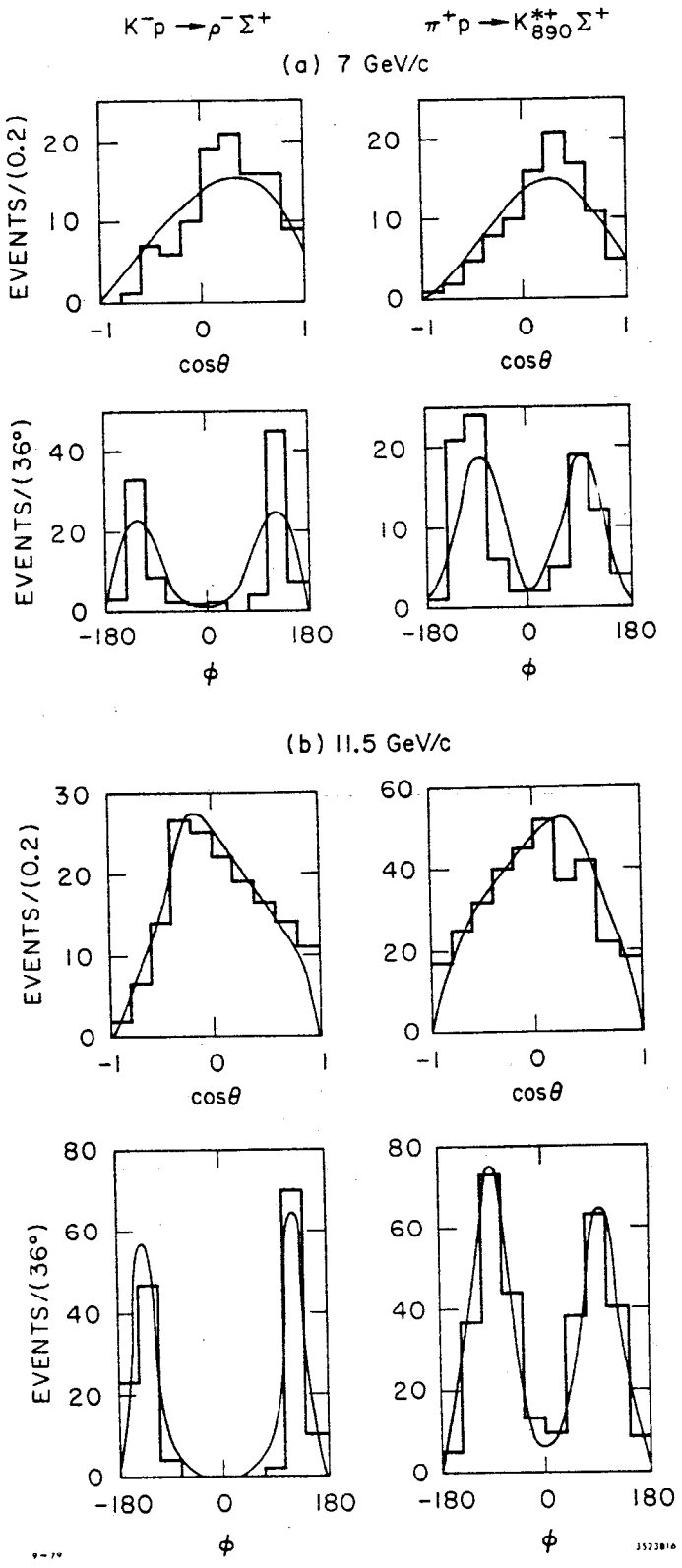
$K^-p \to \rho^-\Sigma^+$
$\pi^+p \to K^{*+}_{890}\Sigma^+$
(a) 7 GeV/c
EVENTS/(0.2)
cosθ
EVENTS/(36°)
φ
(b) 11.5 GeV/c
EVENTS/(0.2)
cosθ
EVENTS/(36°)
φ

Fig. 8

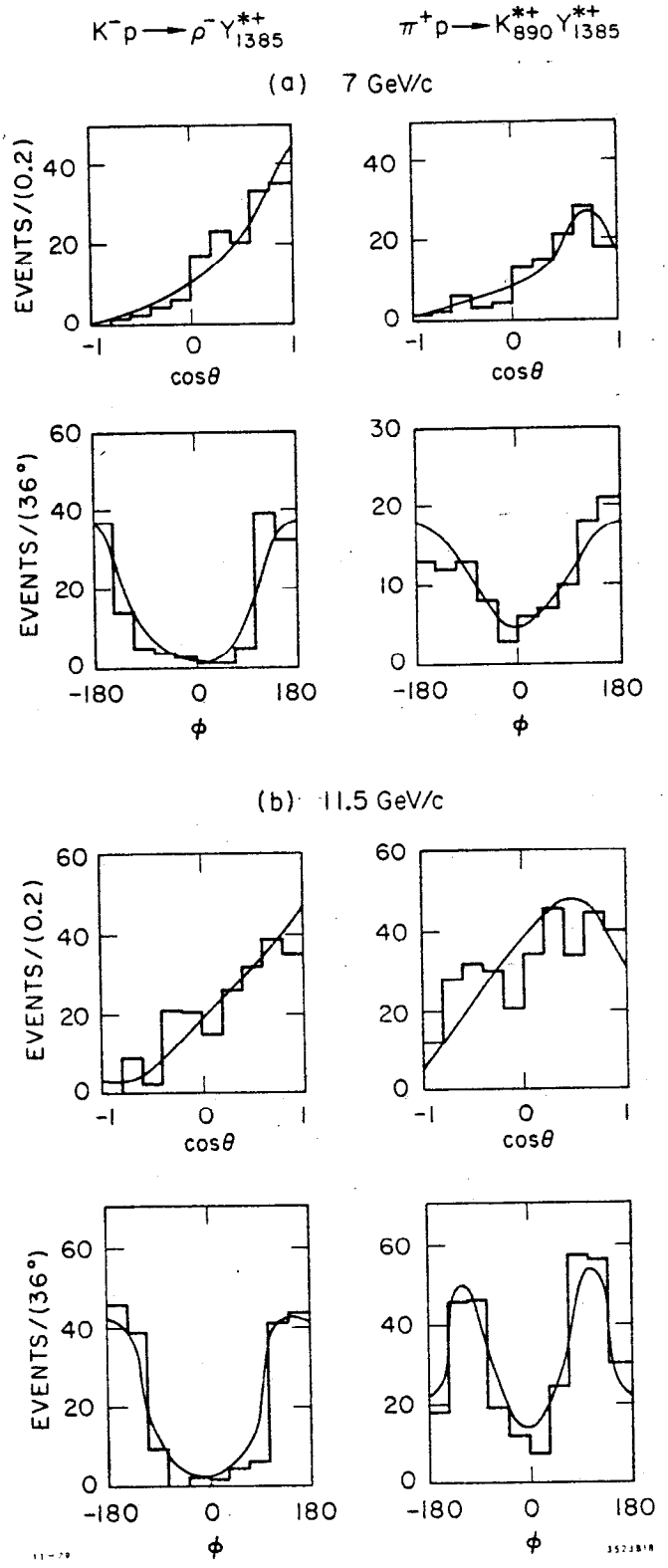
$K^- p \rightarrow \rho^- Y^{*+}_{1385}$
$\pi^+ p \rightarrow K^{*+}_{890} Y^{*+}_{1385}$
(a) 7 GeV/c
EVENTS/(0.2)
cosθ
EVENTS/(36°)
φ
(b) 11.5 GeV/c

Fig. 9

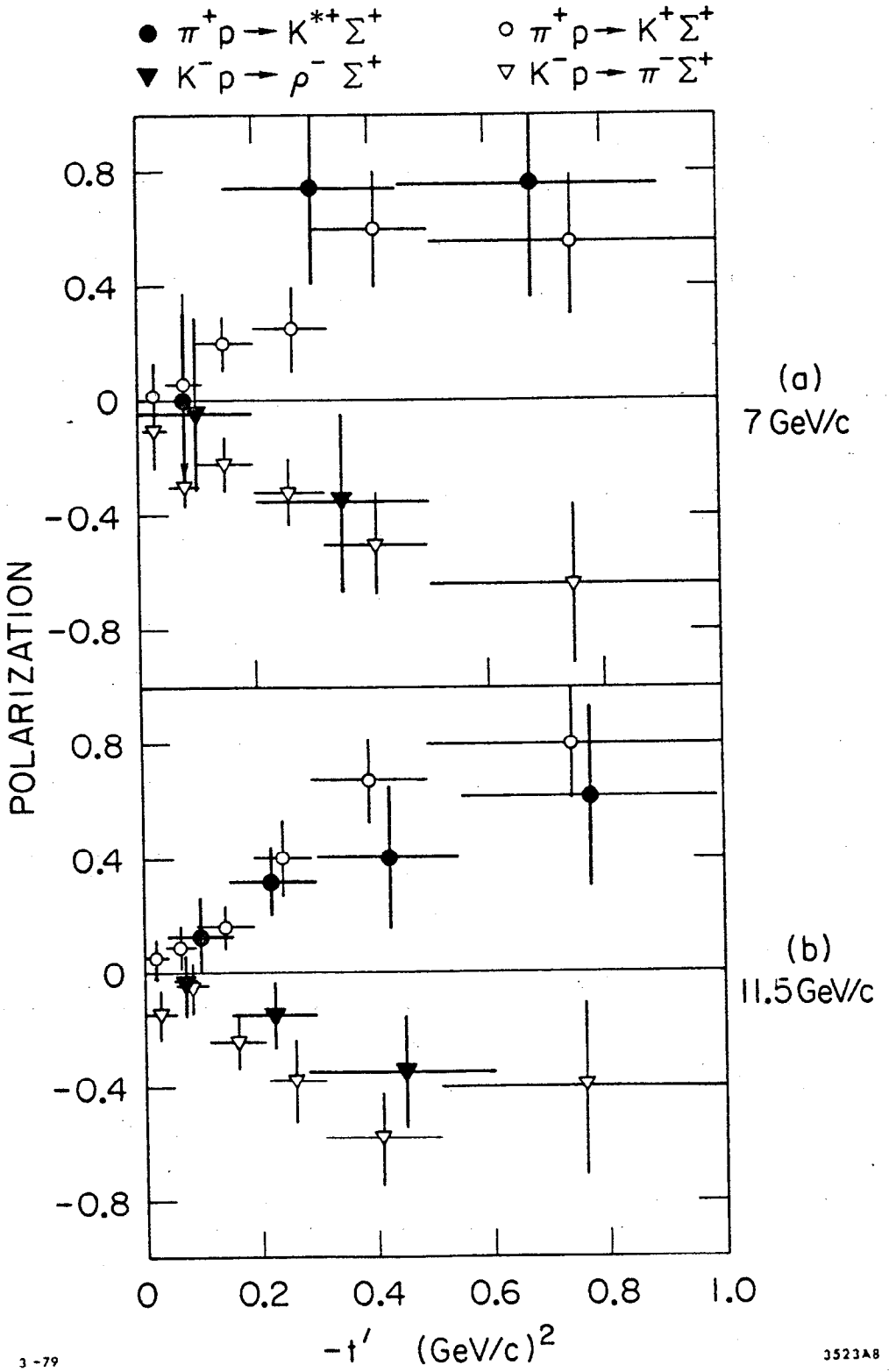
● $\pi^+ p \to K^{*+}\Sigma^+$
○ $\pi^+ p \to K^+\Sigma^+$
▼ $K^- p \to \rho^- \Sigma^+$
▽ $K^- p \to \pi^-\Sigma^+$
POLARIZATION
0.8
0.4
0
-0.4
-0.8
(a)
7 GeV/c
(b)
11.5 GeV/c
0
0.2
0.4
0.6
0.8
1.0
$-t'$ (GeV/c)^2
3-79
3523A8

Fig. 10

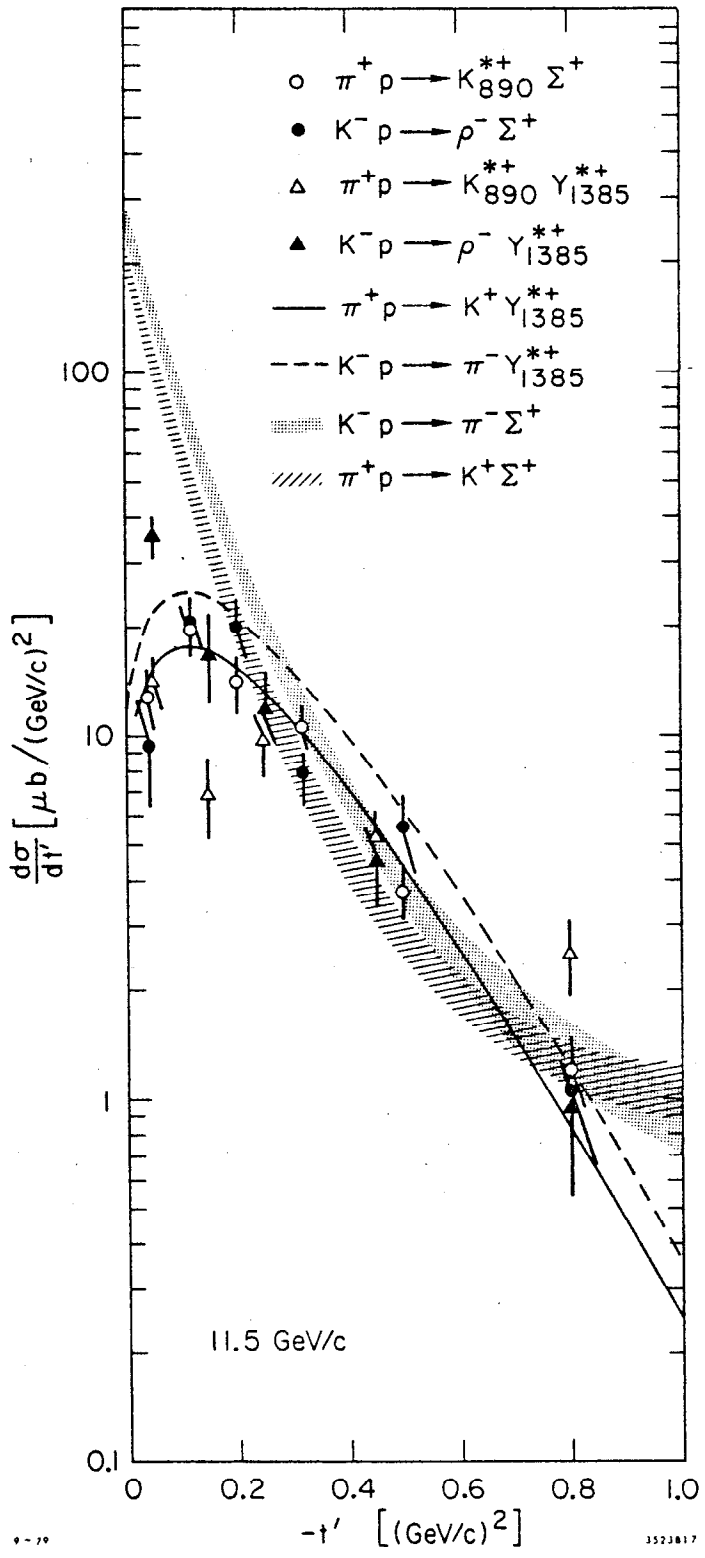
$\pi^+ p \rightarrow K^{*+}_{890}\, \Sigma^+$
$K^- p \rightarrow \rho^-\, \Sigma^+$
$\pi^+ p \rightarrow K^{*+}_{890}\, Y^{*+}_{1385}$
$K^- p \rightarrow \rho^-\, Y^{*+}_{1385}$
$\pi^+ p \rightarrow K^+ Y^{*+}_{1385}$
$K^- p \rightarrow \pi^-\, Y^{*+}_{1385}$
$K^- p \rightarrow \pi^-\, \Sigma^+$
$\pi^+ p \rightarrow K^+ \Sigma^+$
100
10
1
0.1
$\frac{d\sigma}{dt'}\,[\mu b/(GeV/c)^2]$
11.5 GeV/c
0
0.2
0.4
0.6
0.8
1.0
$-t'\ [(GeV/c)^2]$

Fig. 11

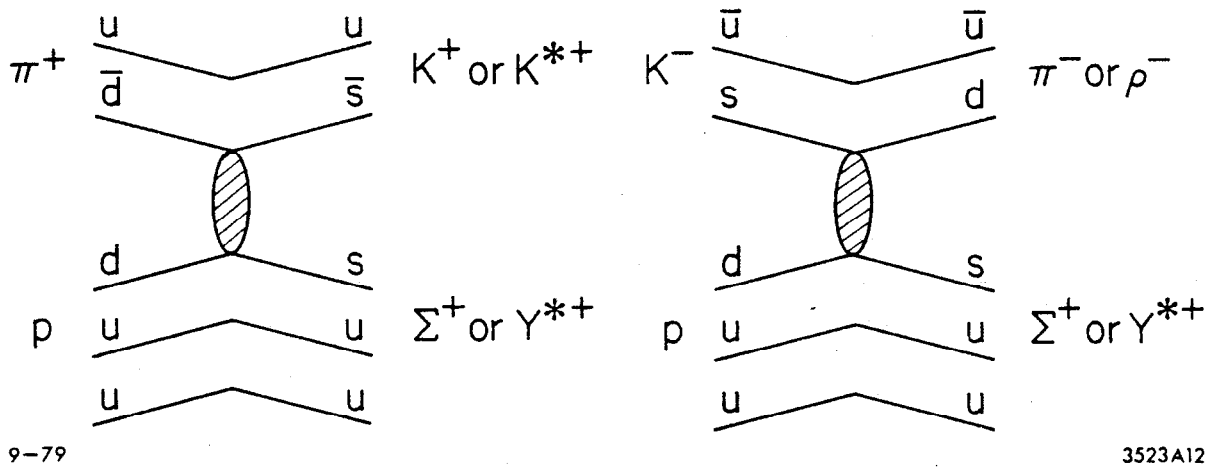
π+
u
d̄
d
p
u
u
u
u
s̄
s
u
u
K+ or K*+
Σ+ or Y*+
K−
ū
s
d
p
ū
d
u
u
u
d
s
u
u
π− or ρ−
Σ+ or Y*+
9–79
3523A12

Fig. 12